CLM-R281

CLM-R281

The impurity control limiter experiment

G. F. Matthews
S. J. Fielding
G. M. McCracken
D. J. H. Goodall
C. S. Pitcher
P. C. Stangeby
J. Allen
R. Barnsley
R. C. Bissel
N. Hawkes
J. Hugill
P. C. Johnson
L. N. Khimchenko
A. M. Ternopol

UK ATOMIC ENERGY AUTHORITY

Culham Laboratory

CLM-R281

The impurity control limiter experiment

G F Matthews, S J Fielding, G M McCracken, D H J Goodall,
C S Pitcher*, P C Stangeby*, J Allen, R Barnsley**, R C Bissel,
N Hawkes, J Hugill, P C Johnson, L N Khimchenko***, A M Ternopol****

Culham Laboratory, Abingdon, Oxon OX14 3DB, UK
(Euratom/UKAEA Fusion Association)

* Institute of Aerospace Studies, University of Toronto, Canada
** Department of Physics, University of Leicester, Leicester, UK
*** Kurchatov Institute, Moscow, USSR
**** Physicotechnical Institute, Kharkov, USSR

ABSTRACT

In this paper we present results from the impurity control limiter experiment (ICL), which was installed on the DITE tokamak. The ICL was designed so that the majority of ions leaving the plasma strike the undersides of its graphite tiles which are angled towards the wall. Our experiments confirm that the impurities sputtered from the ICL are ionised predominantly in the scrape-off layer and that there is significant deposition of neutral carbon on the walls. Both the spatial distribution of ionisation and the toroidal distribution of the carbon on the walls are in good agreement with code predictions. Insertion of the ICL resulted in a 50% reduction of the total radiation in helium discharges and a 10% reduction in the loop voltage when compared with rail limiters of conventional geometry. In deuterium the reduction in the total radiation was only 20% and this is attributed to the greater importance of the wall sources of carbon and oxygen in deuterium plasmas relative to those in helium.

Culham Laboratory
United Kingdom Atomic Energy Authority
Abingdon
Oxfordshire OX14 3DB

November 1987

ISBN: 0 85311 165 0
C/18 Price: £5.00
Available from H.M. Stationery Office

1. INTRODUCTION

In this paper we review the results from the impurity control limiter experiment (ICL), which was installed on DITE in January 1987. Our aim is to describe in detail all the diagnostic data which were obtained during the period of operation. Some of the information which will be presented is not directly relevant to an evaluation of the performance of the ICL. However, we hope that it will provide a useful data base for future reference.

Conventional limiters are usually designed to maximise their power handling capability. Since the power flux in a tokamak is substantially directed along the magnetic field, this is achieved by smearing out the incident power over surfaces at grazing angles to the toroidal magnetic field. The curved cross-section of such a limiter is shown schematically in figure 1(a). An inevitable consequence of this geometry is that neutral impurities which are sputtered from the limiter surfaces will be directed onto closed field lines, where most of them will be ionised. Consequently, conventional limiters tend to create the maximum possible impurity source in a part of the edge plasma where the impurity confinement is better than in the scrape-off layer.

Unlike a conventional limiter, the ICL is toroidally concave on the side facing the plasma, as shown in figure 1(b). It is designed so that the

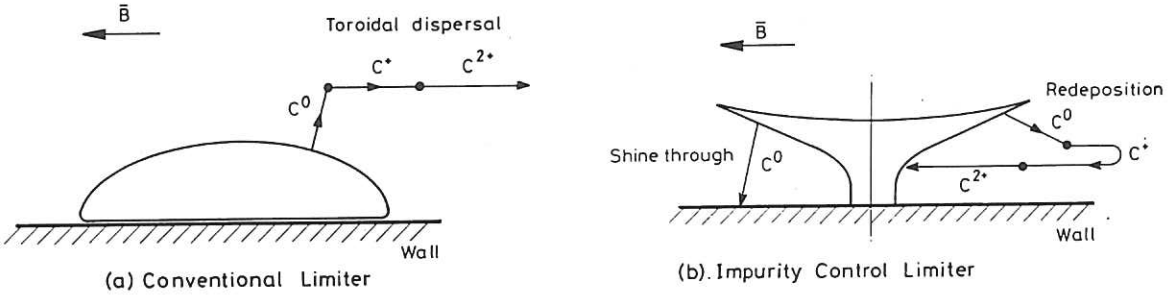

Fig. 1 Schematic of alternative limiter geometries. (a) The conventional limiter which directs impurities onto closed flux surfaces. (b) The ICL which controls impurities by improved screening and shine through.

majority of the incident ions strike the surfaces of its carbon tiles which face away from the plasma. Impurities sputtered from these surfaces are directed towards the walls and have a low probability of ionisation. Furthermore, the ionisation which does occur is strongly localised in the scrape-off layer (SOL). Impurity ions originating in the SOL are more

likely to be driven back to the limiter due to friction with the hydrogenic ions. As a result of these two effects not only is the absolute magnitude of the impurity source reduced, but it is better screened from the main plasma. The ICL was designed on the basis of quantitative predictions made using a two dimensional computer code which models the sputtering and ionisation of carbon from a limiter of arbitrary geometry [1]. These calculations showed that significant reductions in the carbon impurity content of the main plasma were achievable in situations where sputtering from the limiters is the dominant source of contamination.

Superficially the ICL looks rather like a pumped limiter but without the normal throat and pumping arrangements [2]. Pumped limiters have usually been designed with the throat set back at least one power e-folding length from the leading edge of the device but since the e-folding length for the particle flux is generally longer than this, adequate pumping ($\sim$ 10%) is still achieved. If the ICL had been designed this conservatively it would not have worked since most of the physical sputtering occurs within one power e-folding length of the leading edge of the limiter. A further necessary condition for the effectiveness of the ICL, which has not been achieved with most pumped limiters, is that the arc length is sufficient for it to act as the main limiter of the tokamak.

There were three main objectives for the ICL programme. The first was to demonstrate that the detailed predictions for the sputtering and ionisation of the carbon in the vicinity of the ICL were correct. Our second was to demonstrate global effects resulting from the reduced impurity influx. Finally, we aimed to achieve a better understanding of the importance of the limiter impurity source relative to that originating from the walls.

2. THE EXPERIMENT

The ICL consisted of a 180° poloidal sector of 21 cm radius made from 9 Poco-graphite tiles. A schematic diagram of one of these tiles is presented in figure 2 (a). This also shows two of the twelve graphite Langmuir probes which were built into the limiter. The tiles were deliberately made concave on the side facing the plasma so that the toroidal curvature, which is greatest on the outer mid-plane, does not result in plasma contact with the centre of the tiles. Significant global impurity control was only likely to be observed if most of the energetic plasma ions leaving the main DITE plasma were to strike the backward facing surfaces of the ICL. The radius of the ICL was therefore chosen to be 21 cm to minimise the plasma interaction with the main DITE ring limiter which had a radius of 26 cm. The reason for choosing a 180° sector, rather than a full poloidal ring, was to enable the complete withdrawal of the ICL from the torus.

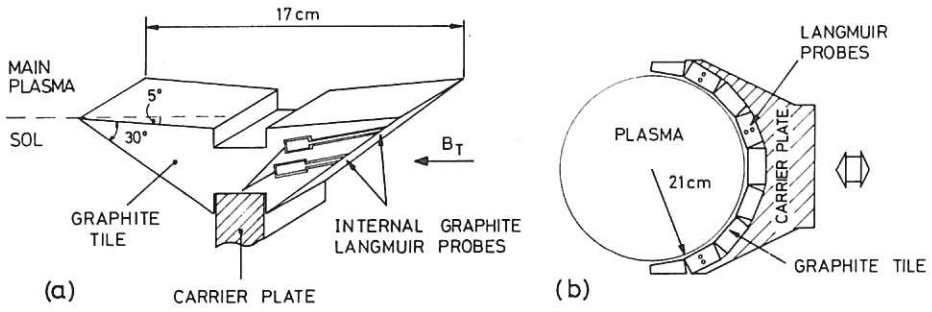

Fig. 2 The ICL. (a) Section through an instrumented tile. (b) Tile locations.

The ICL was mounted on a drive system located at module 3/4; this is shown in figure 3. Also shown in figure 3 are the diagnostics which were used in the investigation of the local physics of the ICL. Twelve Langmuir probes were mounted in three of the tiles, four per tile at two minor radii (5 mm and 20 mm from the leading edge). Each probe consisted of a 3 mm graphite rod which is flush with the surface of the ICL. All the insulators were set well back from the plasma and screened from any deposition of neutral carbon by a collar machined into the probe shaft. Excellent arrangements were available for studying the ICL with CCD cameras equipped with interference filters. The two windows on the rear of the drive tank provided a toroidal view extending out to the leading edges of the ICL. The top of these windows was occupied by a CCD camera and the bottom by an infrared (IR) camera. In order to provide a radial and toroidal picture of the light emission, a miniature CCD camera was mounted in a probe drive on the top of module 3/4. The drive system was required to give an adequate field of view which was otherwise restricted by the port.

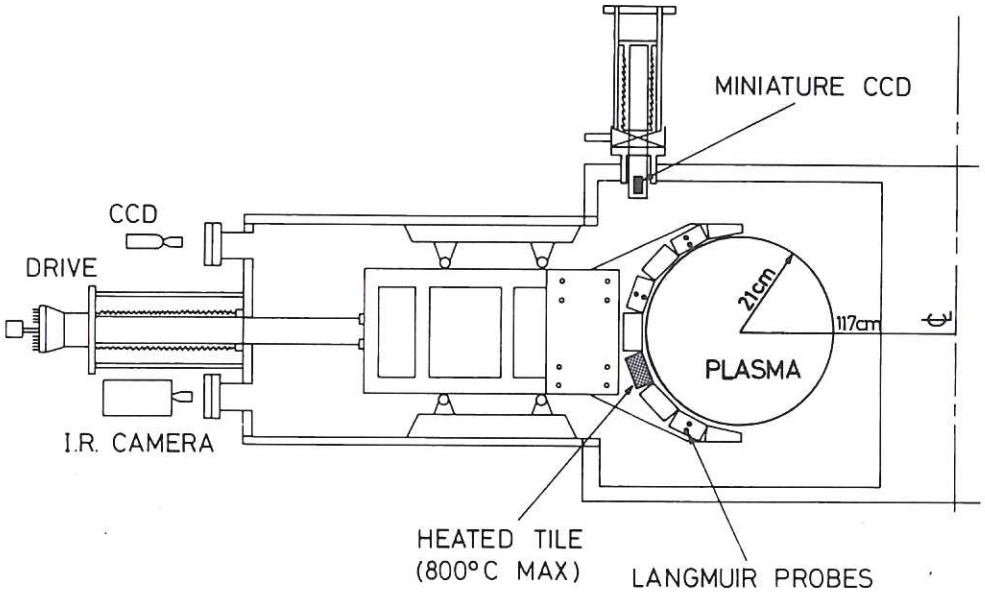

Fig. 3 ICL drive and local diagnostics.

Calibration of both the CCD cameras and the IR camera was made possible by a pair of pyrolytic graphite heaters [3] mounted in tile 5. A maximum bulk temperature of 800°C was achieved in this way. Thermal data was collected by thermocouples mounted in tiles 1,5 and 9. This was recorded during calibration tests and routinely after each tokamak pulse using the DITE thermal SADA which was thus able to estimate the total energy deposited on the ICL.

The toroidal disposition of the ICL and various DITE diagnostics is shown in figure 4. This also shows the location of the rail limiters which were used for comparisons with the ICL. These limiters are mounted on drives on the top and bottom slots of module 15/16. They have a conventional section with chamfer of 15° at the leading edge. When driven in to a radius of 21 cm the rails were in the field of view of a CCD camera mounted on a tangential port on an adjoining module. This complemented the tangential view of the ICL and allowed comparative studies of the radial distributions of the sputtered impurities. Although the rail limiters were not equipped with internal Langmuir probes, scrape-off layer parameters could be measured using the reciprocating probe systems which give complete radial profiles in a single shot.

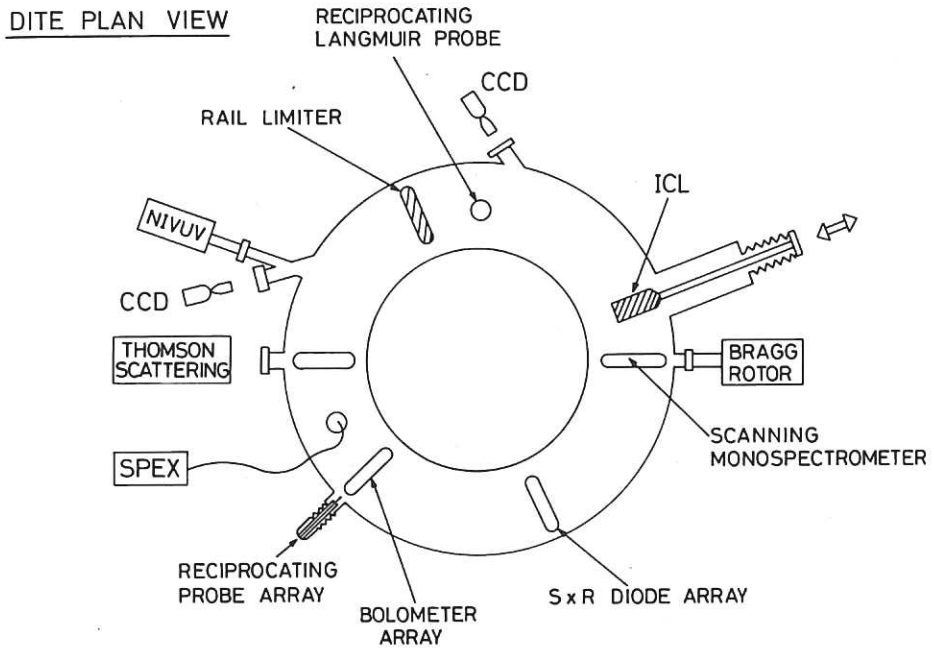

Fig. 4 Plan view of DITE diagnostics.

3. RESULTS: Global Behaviour

Comparisons were made between the rail limiters and the ICL in both deuterium and helium plasmas. The standard conditions used were: a plasma current of 100 kA and a toroidal magnetic field of 2T (q(21cm) = 3.8). Some additional measurements were made at a plasma current of 150kA.

3.1 Radiation

The total radiation from the DITE plasma was measured by integration of the data from the 16 channels of the bolometer array. Non-uniform spacing of the bolometer channels improves the resolution of the array near the edge of the plasma to 2.5 cm. This measurement was adopted instead of the single wide angle bolometer result which appeared to underestimate the radiated power in rail discharges which frequently had radiation profiles which were peaked on the inside of the plasma (MARFEs).

In helium discharges the ICL reduced the total radiated power (P_R) to one half of that seen with the rails at all line average densities. In addition the loop voltage, which is plotted in figure 7(a), fell by 10% (from 2 V to 1.8 V at $n_e = 3 \times 10^{19}$ m^{-3}), consequently reducing the ohmic input power (P_{OH}) by the same amount. The radiated fraction P_R/P_{OH}, which

is plotted in figure 5 as a function of line average density $\bar{n}_e$, is 45% lower with the ICL than with the rails in helium plasma. Despite the significantly lower total radiation in the ICL discharges the disruptive density limit was only increased by a few percent.

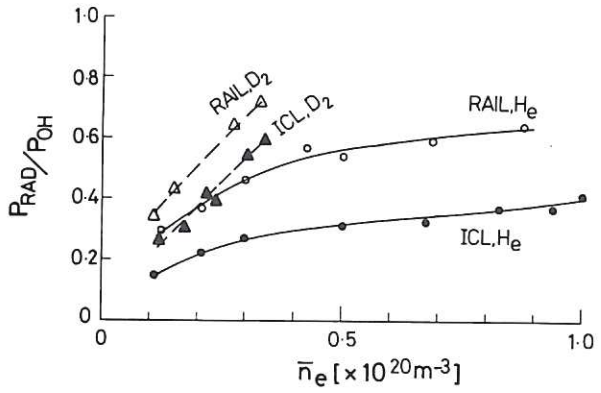

Fig. 5 Density scaling of radiated fraction P_R/P_{OH}.

In deuterium the reduction in total radiation achieved by the ICL is less dramatic than for helium. Also, the disruptive density limit for deuterium is almost three times lower than for helium. The radiated power is higher in deuterium at a given line average density than in helium and increases more rapidly with this parameter. In deuterium the loop voltage is higher and is only decreased by 4% (from 2.3 V to 2.2 V at $\bar{n}_e = 3 \times 10^{19}$ m^{-3}) when the change is made from the rail limiters to the ICL.

Abel inversion of the data from the bolometer array data provides a rough picture of the radial distribution of the radiated power. Radially integrated power is plotted as a function of minor radius in figure 6 for a representative range of line average densities. The algorithm used in the calculation of these profiles takes into account the Shafranov shift of the circular flux surfaces. However, the inversion procedure must of necessity make assumptions about the cylindrical symmetry of the flux surfaces and so can be significantly in error when MARFEs are present. We have therefore selected profiles which minimised this problem. At least half of the total radiation would appear to come from the outer region of the plasma ($r > 15$ cm). The radiation profiles in deuterium and helium are similar in shape but the total power is greater in deuterium.

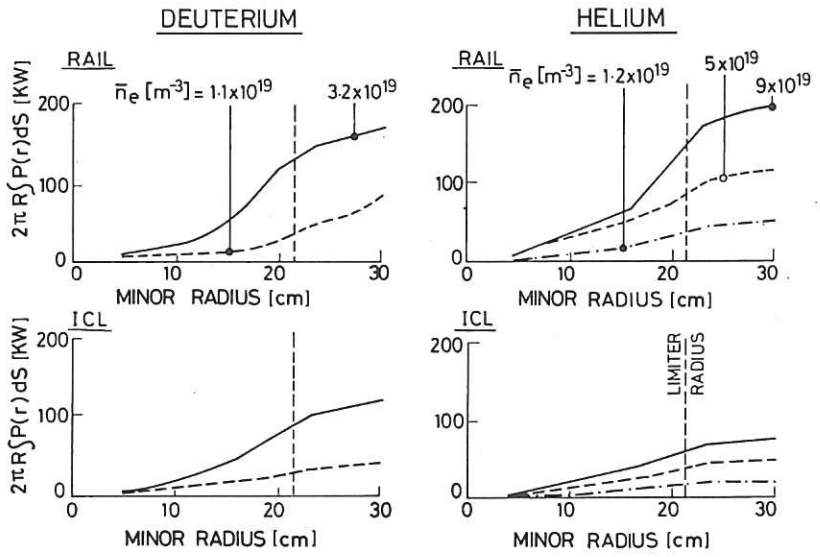

Fig. 6 Radially integrated radiated power versus radius.

3.2 Loop Voltage, Poloidal Beta and Z_{eff}

As mentioned in the last section the ICL discharges had a lower loop voltage (V_L) than an equivalent rail limiter discharge. Figure 7(a) shows that in all cases V_L increased gradually with line average density and that in deuterium it was higher than in helium.

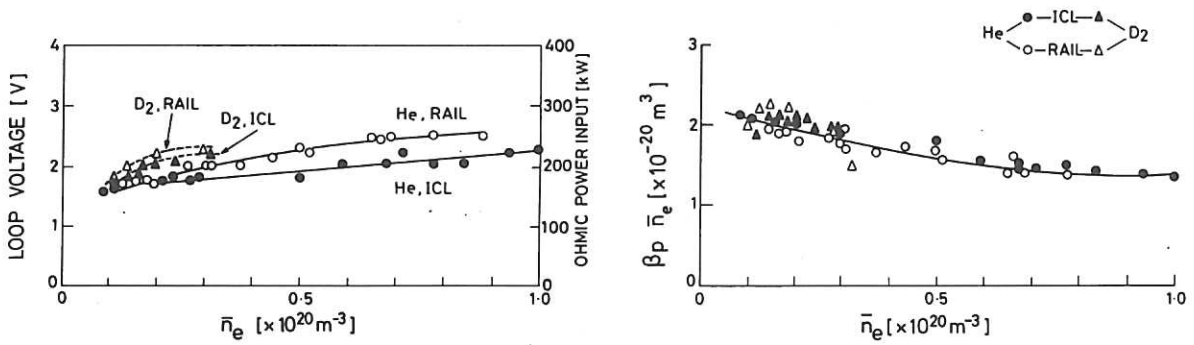

Fig. 7 (a) Loop voltage V_L and (b) normalised poloidal beta $\beta_p/\bar{n}_e$ versus line average density.

An estimate of the effective charge, Z_{eff} can be obtained from the loop voltage if the temperature and density profiles are known. The Thomson scattering system is a single point diagnostic involving fairly large statistical errors and therefore a large number of discharges were required to build up the data set. Profiles were recorded in helium and deuterium plasmas at line average density of 3 x 10^{19} m^{-3} and at a higher density of 7.5 x 10^{19} m^{-3} in helium. At each condition measurements were made with the ICL and rails. The experimental profiles were then fitted with curves of the general form,

$$T_e(\sigma) = T_e(a) + (T_e(o) - T_e(a))\ (1 - (\sigma^2/a^2)^m)^n$$

where σ is the minor radius of the flux surface, a the limiter radius, $T_e(0)$ is the central electron temperature, $T_e(a)$ the electron temperature at limiter radius a, and m and n determine the profile shape. A parabolic function is assumed for the displacement of the centres of the circular flux surfaces and gives the following equation for σ.

$$\sigma = (1 - (1 - \frac{4\Delta}{a^2}\ (R - R_o - \Delta))^{\frac{1}{2}})\ \frac{a^2}{2\Delta}$$

where R is the major radius and Δ is the displacement of the flux surface of zero radius from the geometric axis of the machine which is at R_o. Fitted parameters for each profile studied are listed in table 1(a).

In figure 8(a) and 8(b) we have plotted the Thomson scattering data for the high density helium discharge and the fitted curves for each case studied. The temperature profiles recorded in the three discharge types are very similar, it seems to make little difference whether it is low or high density, deuterium of helium. A comparison of the rail limiters with the ICL at each condition shows that the profiles are almost identical. However, if the temperature profile shape is indeed fairly constant then the gradual decline in the value of $\beta_p/\bar{n}_e$, shown in figure 7(b) implies that the temperature should fall as the density rises provided that the density profile does not show any dramatic change.

An analysis of these profiles has been carried out using a one-dimensional code which as been applied to previous DITE data [4]. This calculation calculates the current profile using the Spitzer resistivity and also applies the corrections due to neoclassical theory. The bulk parameters which the code predicts are the effective charge Z_{eff}, the electron poloidal beta β_e and the q on axis q_o. We have listed these parameters in table 1(b) along with experimental values where relevant. The neoclassical correction changes the value of Z_{eff} by no more than 6%.

In helium there is a clear reduction in Z_{eff} when the ICL replaces the rail limiters. However, with a deuterium plasma the change is very small. The computed electron poloidal beta β_e is in reasonable agreement with the β_p measured with the diamagnetic loop: the contribution from the ions is

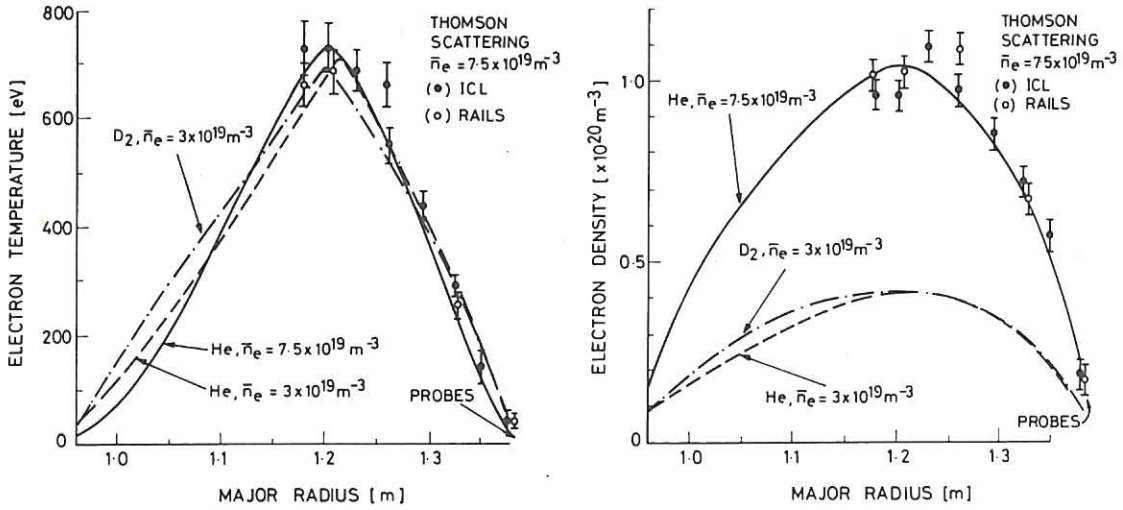

Fig. 8 Radial profiles of (a) electron temperature and (b) electron density measured with the Thomson scattering system.

Table 1

(a) Fitted profile

Gas	$\bar{n}_e$ [$\times 10^{19}$ m^{-3}]	Δ [m]	Density Profile $n_e(o)$ [$\times 10^{-19}$ m^{-3}]	$n_e(a)$ [$\times 10^{-19}$ m^{-3}]	m	n	Temperature Profile $T_e(o)$ [eV]	$T_e(a)$ [eV]	m	n
D_2	3.0	0.030	4.13	0.74	1.10	0.914	698	15	0.492	0.836
He	3.1	0.044	4.16	0.88	0.93	1.04	713	37	0.54	1.11
He	7.3	0.034	10.4	1.4	0.76	0.73	731	19	0.72	1.63

(b) Calculated values of Z_{eff} and β_e based on the Thomson scattering profiles. Zeff (spec) is derived from the spectroscopic data of section 4 (O, C, Fe).

Gas	Limiter	$\bar{n}_e$ [$\times 10^{19} m^{-3}$]	V_L (Exp)	Z_{eff}	Z_{eff} (Spec)	β_e	β_p (Exp)	q_o
D_2	RAIL	3.0	2.55	5.13	2.77	0.45	0.56	1.11
	ICL		2.52	5.05	2.76			
He	RAIL	3.1	2.10	3.48	2.86	0.44	0.48	0.95
	ICL		1.68	2.50	2.61			
He	RAIL	7.3	2.64	4.77	2.74	1.03	1.2	0.90
	ICL		2.22	3.74	2.59			

unlikely to be more than 20% particularly in helium where the ion density is half the electron density. The main source of error here is the uncertainty in the profile shape which results from the lack of diagnostic information from the inner half of the temperature profile.

3.3 Power and Energy Balance

In the past the energy balance on DITE has been investigated using the data gathered from thermocouples mounted inside the limiters and thermistors located on the bellows sections of the torus. The integrated energy calculated in this way could then be compared to the difference between the ohmic input energy and the radiated energy obtained through time integration of the bolometer data. This inventory has been repeated for the ICL but with additional information available from the internal Langmuir probes.

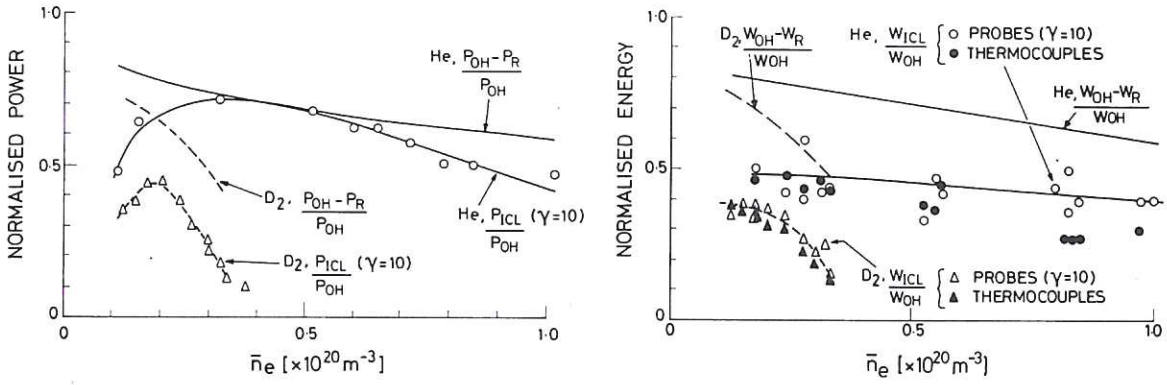

Fig. 9 (a) Comparison of the normalised convected power determined by the ICL probes with the difference between the ohmic input and radiated powers. (b) Comparison of the normalised energy recorded by the ICL thermocouples with the ICL probes and the difference between input and radiated energies.

In order to calculate the power arriving at the ICL from the probe data we had to assume a value for the power transmission factor of the sheath δ. The power arriving at any point on the ICL surface is given by the product $\delta J_{sat} T_e$, where J_{sat} is the saturated ion current density and T_e the local electron temperature. We took a constant value of $\delta = 10$. The total power arriving at the ICL is then calculated by integration of the power profile at each poloidal position where it is measured and by multiplying this quantity by a poloidal arc length over which this power is assumed to be constant. Total energy is simply obtained by time integration of the power over the full discharge duration. In figure 9(a) the convected power

fraction is plotted as a function of line average density in both deuterium and helium plasmas. This is compared with the difference between the ohmic input power and the total radiated power from the bolometer array. The power accounting in the helium plasmas appears reasonable at medium and high density and is worse at low density. In deuterium a significant fraction of the power is unaccounted for particularly near the density limit.

Our assumption that the energy transmission factor $\delta = 10$ is well supported by the data for the energy inventory which is plotted in figure 9(b). This shows that there was very good agreement between the deposited energy measured with the thermocouples and that calculated from the probe data. As with the power we again have a problem in accounting for all the energy and the situation is somewhat worse in deuterium than in helium. Although we do not get absolute agreement between the measured energy deposited on the ICL and that implied by the difference between the ohmic input and radiated energies, there is good qualitative agreement in terms of the density dependence. The energy deposited on the 26 cm DITE ring limiters was negligible and the energy recorded by the thermistors located on the bellows sections was in reasonable agreement with the radiated energy from the bolometer array.

3.4 Recycling and Pumping

A radial and poloidal integration of the ion saturation current recorded by the internal probes gives a measure of the total ion current I_{ion} arriving at the ICL. This is presented as a function of line average density in figure 10(a) for both deuterium and helium plasmas. Since most of the ions incident on the limiter are recycled a much smaller current of fresh gas

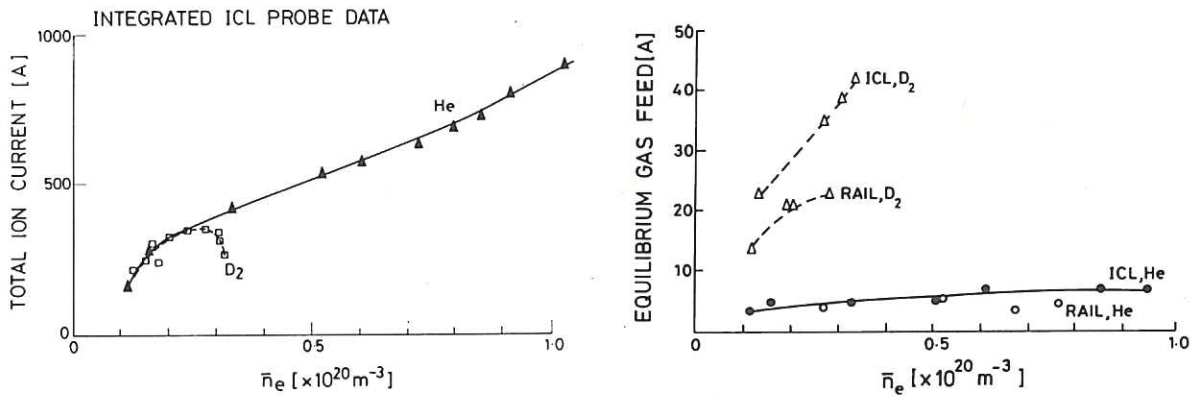

Fig. 10 (a) Total ion current to the ICL and (b) gas feed current (amps of electrons) required for density equilibrium, versus line average density

I_{gas} is required to maintain the line average density. In figure 10 (b) we have plotted the gas feed current, in amps of electrons, required for density equilibrium.

The recycling coefficient for the equilibrium state is simply $R = (I_{ion} - \eta I_{gas})/I_{ion}$, which is tabulated in table 2 for a variety of conditions and assuming that the total ion flux to the rail limiters equals that to the ICL. The gas utilisation efficiency η is assigned a value of unity in all cases. This will introduce an error which is difficult to quantify since η depends on the precise condition of the walls in the vicinity of the gas feed.

Table 2

Recycling Coefficient

$\bar{n}_e$ [$\times 10^{20} m^{-3}$]	D_2		He	
	RAIL	ICL	RAIL	ICL
0.12	0.93	0.89	0.98	0.98
0.28	0.93	0.90	0.99	0.99
0.85	-	-	-	0.99

It will be apparent from this data that the recycling coefficient for helium plasmas is nearly unity under all conditions. This is consistent with the fact that helium is not trapped by the carbon limiters and so has no natural sink. Deuterium on the other hand has a recycling coefficient which is significantly less than unity due to trapping of ions in the carbon limiters and charge exchange particles in the walls. These reservoirs are sufficiently large that they show no sign of saturating during the 600 ms duration of a typical DITE discharge. The recycling coefficient is slightly lower in an ICL discharge than in the equivalent rail limiter case. If we think of it in terms of a pumping efficiency then the ICL would apear to "pump" an additional 3% to 4% of the total ion current leaving the plasma. During the density rise phase of the discharge this figure is significantly higher but soon saturates.

3.5 Soft X-ray Emission

Data was collected with the top array of the DITE soft X-ray diode system. This array consists of 21 surface barrier diodes located behind mylar

foils 6 μm thick, sensitive to x-rays of energy > 1keV. The intensity of the central channel of this array normalised to the line average density is plotted in figure 11(a). There is a significant difference between the rail limiter and ICL results. In both helium and deuterium plasmas the soft X-ray emission is lower with the ICL; the greatest difference occurs at low density and the curves converge at the density limit. This behaviour is very similar to that of the Fe XVII line intensity, see figure 14, and it therefore seems reasonable to ascribe the majority of the soft X-ray emission to the iron impurity.

Although the absolute level of the soft X-ray emission is substantially reduced by the insertion of the ICL, the normalised profile, shown in

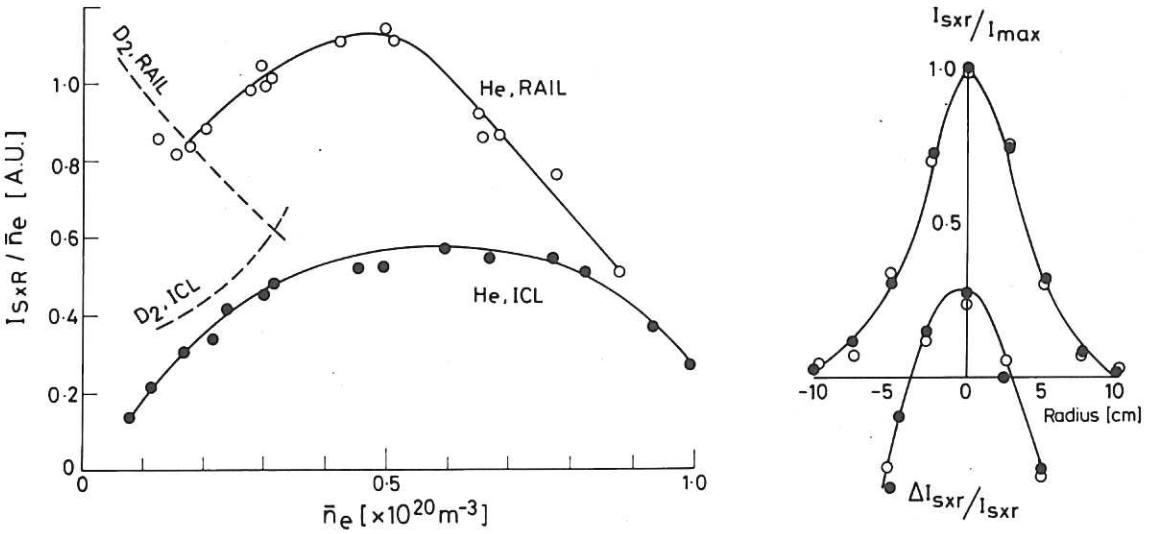

Fig. 11 (a) Central soft X-ray channel vs $\bar{n}_e$. (b) Normalised SXR signal and sawtooth amplitude versus radius.

figure 11(b), is unaffected. Also shown in this figure is the radial dependence of the normalised sawtooth amplitude which again shows no significant difference between rail and ICL discharges.

4. SPECTROSCOPIC MEASUREMENTS

A wide range of spectrometers were used to assess the performance of the ICL. The locations of these instruments on the DITE tokamak are shown in figure 4. The objective of the ICL experiment was to reduce the impurity influx into the confined region of the plasma and hence to effect a

reduction in the core concentrations. The spectroscopic measurements have therefore been aimed at quantifying both the changes in impurity influx and core concentrations of the major impurities when the change is made from the rail limiters to the ICL. In addition an attempt has been made to evaluate the relative magnitude of the impurity influxes from the walls and limiters. If the former were dominant it would substantially reduce the effectiveness of the new limiter.

4.1 Interpretation of the Spectroscopic Data

The majority of the observations were of the central chord line intensity I, for a specific species of charge state z and density n_z. In general this may be written as the integral

$$I = A \int_{-a}^{a} n_e(r)\, n_z(r)\, \langle \sigma v \rangle_{ex}\, dr \qquad 4.1$$

where $\langle \sigma v \rangle_{ex}$ is the excitation rate and A includes the geometric and other constants. All the instruments were absolutely calibrated to give the number of photons detected per unit area of plasma along each line of sight and hence a direct measure of intensity I. The radial impurity ion distribution, $n_e(r)$, is strongly dependent on the ionisation cross-sections which are functions of the electron temperature $T_e(r)$. The impurity transport is also an important factor except in the special case of coronal equilibrium where a knowledge of electron temperature profile is sufficient. In the discharges which we have studied where $T_e(r)$ is independent of the line average density, and the electron density profile shape is also practically invariant, equation 4.1 can be approximated to

$$n_I \propto I/n_e$$

for core impurities, where n_I is an average value of the total impurity density and n_e is the line average density. The accuracy of this approximation depends on the particular spectral line and ionisation state under observation. In the following sub-sections we will consider how well this approximation applies for a range of measurements.

In the following discussions of specific impurities we also present results from a one-dimensionsal impurity transport code which was developed by Behringer [5] in an attempt to account for the lack of coronal equilibrium which is particularly important near the periphery of the plasma. This is the region where the lower ionisation states of the impurities are dominant and where most of the power is radiated. Such a model is therefore

important if any estimate of the total radiated power from all the different charge states of a particular impurity is to be estimated. The code solves the following diffusion equation for each impurity ionisation stage, of density n_z, which includes an empirical inward convective pinch term:

$$-\frac{1}{r}\frac{d}{dr}\left(r D_z \frac{dn_z}{dr} + 2D_z S \frac{r}{a^2} n_z\right) = \text{sources} - \text{sinks}$$

where D_z is the cross-field impurity diffusion coefficient and S a dimensionless peaking parameter. On the right hand side of the equation are the source and sink terms which represent the rate at which ions enter or leave the specific charge state. In the code it is assumed that the impurities are mono-energetic and are launched into the plasma periphery from the wall. The only input data required are the electron temperature and density profiles and the values of S and D_z. In the following sections we apply the code to the three standard profiles described in section 3.2 using a constant value of D_z=0.26 m^2s^{-1} and S=2($\bar{n}_e$=3x0^{19} m^{-3}), S=6($\bar{n}_e$= 10^{20} m^{-3}).

The main impurity ions observed were carbon, oxygen and iron. Carbon is important because the modelling work for the ICL concentrated on the physical sputtering of carbon from the graphite limiters. The oxygen is studied because it is believed to originate from the walls and is characterised by a relatively complex life history involving recycling from the limiters and a variety of chemical reactions while resident on the wall surfaces. Iron is taken to be representative of the metalic impurities which originate from sputtering at the walls and which reach a dynamic equilibrium on the limiter surfaces on which they are deposited and re-sputtered.

4.2 Oxygen

Figure 12(a) is a plot of $I/\bar{n}_e$ for the OVIII line, (IS-2p, 19Å) measured with the Bragg rotor X-ray spectrometer, as a function of $\bar{n}_e$ for four discharge conditions: rail limiters and ICL, deuterium and helium plasmas. Since the OVIII line is emitted from near the plasma core, the coronal equilibrium model might be expected to apply. If this is so then $I/\bar{n}_e$ is proportional to the oxygen impurity content of the plasma. On this basis the ICL can be seen to reduce the oxygen content of the plasma to 80% of that recorded with the rail limiters in both helium and deuterium discharges. A comparison between the deuterium and helium plasmas suggests that the oxygen content in deuterium is twice that in helium. In all cases the oxygen content declines with density.

The OVI line (2S-2p, 1037Å) was observed with the normal incidence vacuum ultraviolet spectrometer (NIVUV) and the measured values of $I/\bar{n}_e$ are plotted in figure 12(b). A comparison with the behaviour of the OVIII shows that the main differences are: firstly, that in deuterium $I/\bar{n}_e$ for OVI increases strongly with density whereas with OVIII it decreases and secondly, that the ICL reduces $I/\bar{n}_e$ for OVI to around 50% of the value seen with the rail limiters, compared with 80% reduction of the OVIII line.

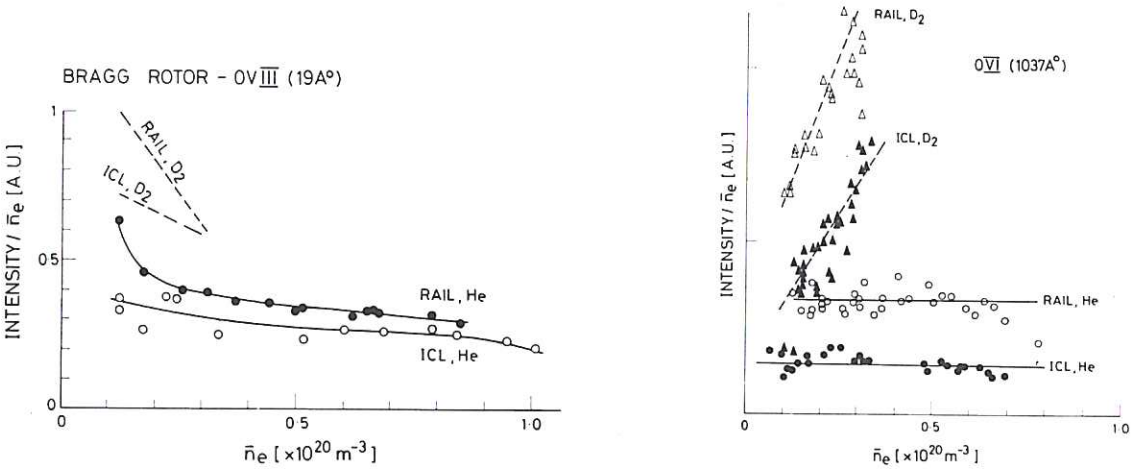

Fig. 12 (a) OVIII (19 Å) intensity measured with the Bragg rotor and (b) OVI (1037 Å) from the normal incidence spectrometer. Both normalised to line average density.

This discrepancy in behaviour means that the assumption of coronal equilibrium and toroidal uniformity does not apply very well to the OVI which as we shall see is emmitted from a shell relatively far from the plasma core.

In table 3 the results from the one-dimensional transport code are presented for the three standard profiles. In order to calculate an absolute value for the central concentration n_o/n_e and total radiated power P_r^o the code result is normalised to the experimentally determined line of sight intensities for either OVIII or OVI. If the code were an accurate representation of reality in both cases then the results from either normalisation would be identical. Although there is reasonable agreement between the predictions for helium plasmas with the ICL limiters, there are still large discrepancies between the OVI and OVIII results for the other conditions. In particular the OVI results suggest that the ICL reduces the total radiation due to oxygen by about a factor of two, whereas the OVIII shows a much smaller effect. Table 3 summaries the results from a comparison of the code with experiments.

Table 3

One-dimensional transport code results for oxygen. Central concentration $n_o/n_e(o)$. Total power radiated P_r^o.

Gas	Limiter	$\bar{n}_e$	OVIII		OVI	
			$n_o/n_e(o)$	P_r^o	n_o/n_e	P_r^o
		[x10^{19}m^{-3}]	[%]	[kW]	[%]	[kW]
D_2	ICL	3.0	1.4	32	7.6	170
	RAIL		1.6	35	12.9	285
He	ICL	3.1	0.7	20	1.1	28
	RAIL		1.0	25	2.2	56
He	ICL	7.3	0.58	17.5	3.06	91.3
	RAIL		0.63	19	7.60	23.1

In addition to the integrated values the one-dimensional transport code predicts the radial distributions of the line radiation and the power radiated per unit volume. An example of this is plotted in figure 13, and since the results are normalised they are qualitatively the same for all the cases modelled. The important features are the peaking of the OVI radiation only 1cm inside the limiter radius and the location of the OVIII near the plasma core. As would be expected the total radiated power summed over all lines is strongly localised in the plasma boundary.

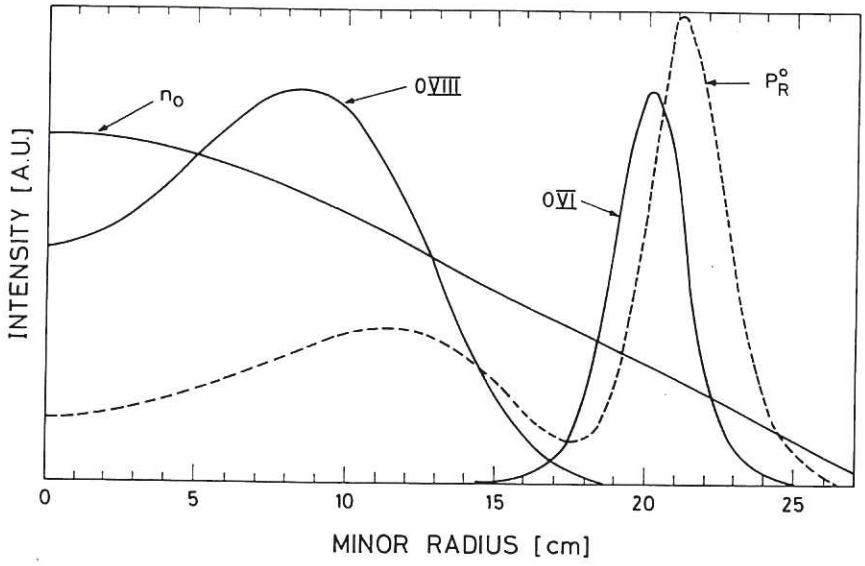

Fig. 13 Code predictions for the radial distribution of the oxygen line radiation and radiated power P_r^o (Helium, $\bar{n}_e = 3\times10^{18}m^{-3}$).

One dimensional calculations based on the OVI observations can be shown to be unreliable through a comparison of the time it takes an O^{5+} to achieve toroidal uniformity, τ_u, with the residence time of the ion τ_r. The time for an ion of charge state z to achieve uniformity is given by

$$\tau_u \approx (2\pi Rq)^2/D_{||}^z$$

where $D_{||}^z$ is the classical parallel diffusion coefficient for the particular combination of impurity ion and background plasma, R is the major radius and q the safety factor at the radius of the peak ion density for the particular charge state. The residence time τ_r is determined by the ionisation process hence

$$\tau_r \approx 1/(n_e\langle\sigma\rangle_{iz})$$

where $\langle\sigma v\rangle_{iz}$ is the ionisation rate coefficient for the ion of charge state z. Taking values of $n_e = 10^{19}$ m^{-3} and $T_e = 150eV$ for an O^{5+} ion then $\tau_u \approx 4ms$ in a helium plasma, $\tau_u \approx 6ms$ in deuterium and $\tau_r \approx 0.5$ ms. At higher density in helium the situation will be worse since τ_r decreases with density whilst τ_u increases. Spatial uniformity will thus not be achieved in any of the cases studied.

4.3 Carbon

Since the ICL and rail limiters used in DITE were graphite, and the original modelling work was based on the physical sputtering of neutral carbon atoms from their surfaces, a careful study of the carbon emission is very relevant to assessing the performance of the ICL. As will be evident from the discussion of the observations of the various oxygen lines, if the interpretation is to be simple it is essential to choose spectral lines which are emitted from a uniform toroidal shell. Ions in high charge states are most likely to fulfil this requirement. To this end an attempt was made to measure the 1s - 2s Lyman α transition in CVI using the Bragg rotor spectrometer but these efforts were unsucessful. This left us with measurements of the CV line at 2271Å using the scanning mono-spectrometer which rapidly sweeps its chord of observation across the plasma minor radius. As will be seen from figure 4 this instrument is mounted on the top of DITE on a slot port on the module adjoining the ICL.

A repeat of the calculations used in evaluating the uniformity of the O^{5+} ions but for C^{4+}, at a plasma density of $n_e = 10^{19}\ m^{-3}$, gives $\tau_u \approx 5ms$ in helium plasmas, $\tau_u \approx 1ms$ in deuterium and $\tau_r \approx 10ms$ for either. We would therefore not expect adequate toroidal uniformity since this will only be achieved if $\tau_u << \tau_r$. If the scanning mono-spectrometer were equidistant toroidally from the rails and the ICL then this could be ignored in making the comparison between the two. Unfortunately this is not the case because the instrument is situated almost on top of the ICL whilst it is 180° away from the rail limiters.

The intensity of the CV line normalised to the line average density is plotted in figure 14. In this case the intensity I represents the chord intensity integrated across the plasma cross-section which is swept by the instrument. This has a different weighting to the central chord line intensity recorded by the other spectrometers. An analysis of the experimental data shows that the ratio between the central chord and the integrated CV signals is approximately constant. This implies that the emission profile of the CV is not very dependent on line average density. The value of $I/\bar{n}_e$ for CV declines rapidly with increasing $\bar{n}_e$ in both deuterium and helium discharges. As with OVIII the ICL reduces the CV intensity, over that with rail limiters, by only 20-30%. An application of the one-dimensional transport code to the CV data gives the estimated total radiation and core carbon concentrations listed in table 4. These figures show that the carbon is of comparable importance to the oxygen in its contribution to the total radiation, and that the carbon content of the deuterium plasma is higher than in helium. However, the calculation still

fails to explain why the total radiation from the ICL discharges in helium is half that of equivalent rail limiter discharges.

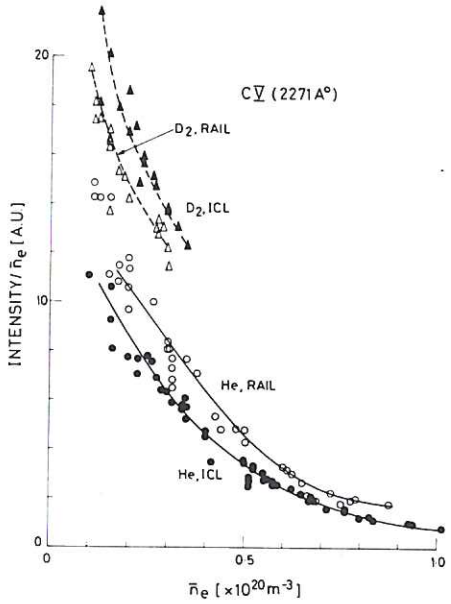

Fig. 14 Radially integrated CV emission (2271Å) from the scanning monospectrometer.

Table 4

One-dimensional transport code results for carbon central concentration $n_c/n_e(o)$. Total power radiated P_r^c.

Gas	Limiter	$\bar{n}_e$ [x10^{19}m^{-3}]	$n_c/\bar{n}_e^{CV}$ [%]	P_r^c [kW]
D_2	ICL	3.0	3.4	36
	RAIL		3.0	31
He	ICL	3.1	1.0	18
	RAIL		1.3	22
He	ICL	7.3	1.2	14
	RAIL		1.7	20

The code also predicts the radial distribution of the CV line emission and this is directly compared with the normalised experimental results in figure 15. Equally good agreement is obtained in each standard discharge.

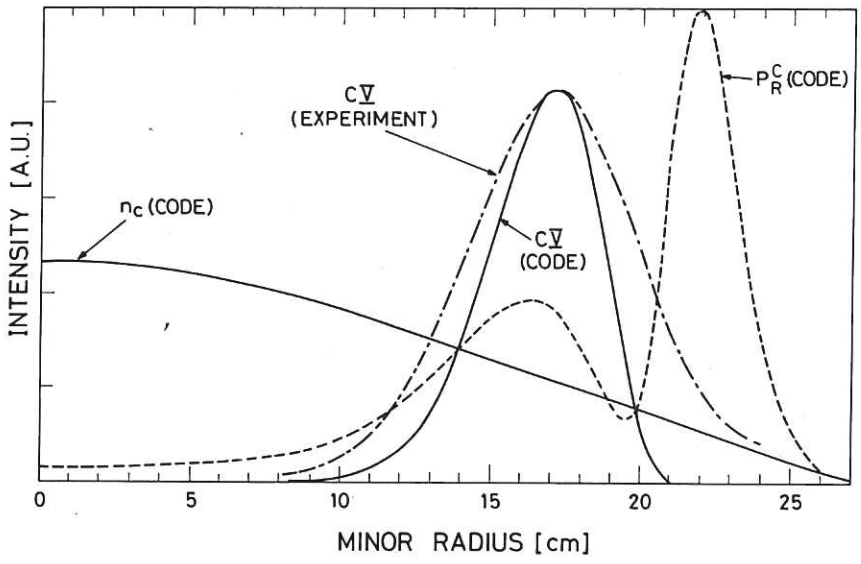

Fig. 15 Comparison of the experimental and predicted radial distributions of the CV emission. Also plotted is the predicted radiated power P_r^C and carbon density n_c (Helium, $\bar{n}_e = 3 \times 10^{18}$ m^{-3}).

Comparisons have been made between the inner and outer halves of the CV profile. Since the ICL is only a 180° sector on the outside of the torus, this is equivalent to comparing regions of plasma with greatly differing connection length to the limiter and hence provides a measure of the toroidal uniformity. The conclusion from this is that toroidal non-uniformity does not seem to explain why a larger reduction in CV is not observed when the ICL replaces the rails in helium.

Measurements of the CIII and CIV line intensities were also made with the NIVUV instrument and had a very similar density scaling to the OVI line, with a halving of intensity when the rail limiters are exchanged for the ICL. However, as with the OVI, these results must be rejected on the grounds of insufficient toroidal uniformity of the emission. Any simple interpretation of this data is very dubious.

4.4 Iron

Iron is the major metallic component of the stainless steel walls of the DITE vacuum vessel and is therefore the major high Z impurity. Measurements of the central chord emission of the Fe XVII line ($2P^6-2P^53d$, 15Å) were made with the Bragg rotor spectrometer and the resulting values of $I/\bar{n}_e$ are plotted in figure 16. This shows that the ICL

can be very effective at reducing the iron emission at low densities in both deuterium and helium plasmas but that it has little effect near the density limit. As has been already mentioned the density scaling of the normalised central soft X-ray intensity, which is plotted in figure 11(a), has a behaviour very similar to that of the Fe XVII.

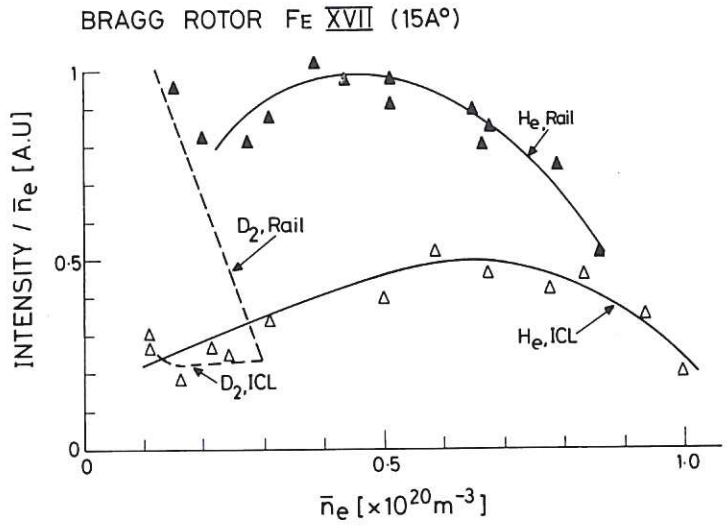

Fig. 16 Fe XVII (15 Å) intensity measured with the Bragg rotor spectrometer and normalised to the line average density.

Using the same background plasma parameters as for oxygen and carbon, the one-dimensional model predicts the spatial distribution of Fe XVII intensity and radiated power shown in figure 17. The Fe XVII line is emitted from near the plasma centre and so will provide a good measure of the iron impurity concentration. In table 5 the calculations show that in all cases the iron concentrations are low and that the iron contributes 10% or less to the total radiation.

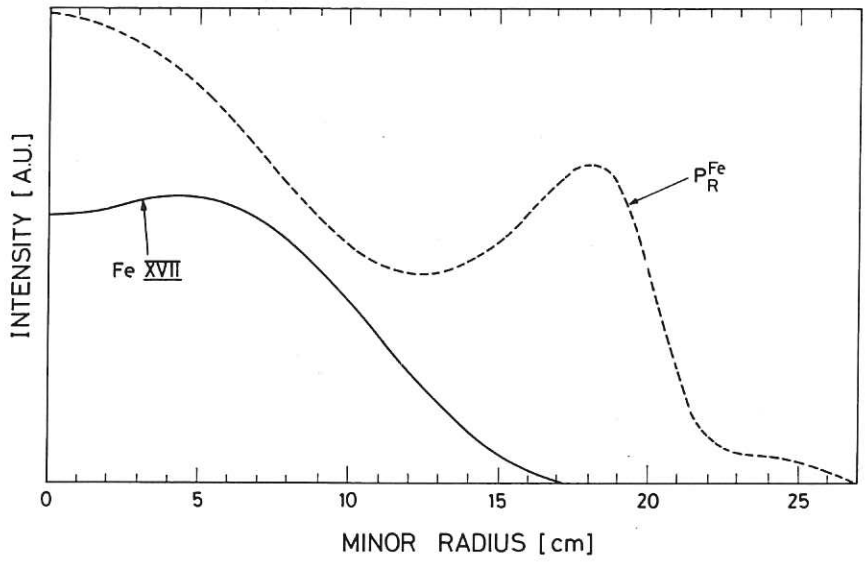

Fig. 17 Code prediction for the radial distribution of the Fe XVII radiation and radiated power P_R^{Fe} (Helium, $\bar{n}_e = 3 \times 10^{18}$ m^{-3}).

Table 5

One-dimensional transport code results for iron central concentration $n_{Fe}/n_e(o)$. Total power radiated P_r^{Fe}.

Gas	Limiter	$\bar{n}_e$ [$\times 10^{19}$m^{-3}]	FeXVII $n_{Fe}/n_e(o)$ [%]	P_r^{Fe} [kW]
D_2	ICL	3.1	0.003	1.0
	Rail		0.002	0.7
He	ICL	3.0	0.007	1.9
	Rail		0.016	4.7
He	ICL	7.3	0.004	3.6
	Rail		0.007	6.2

4.5 The Measurement of Impurity Influxes from the Walls

An area of the DITE vessel wall was viewed with a visible spectrometer at a location remote from either the rail limiters or the ICL, as shown in figure 4. The region of the spectrum selected for study included the lines OII(4350Å), CII(4267Å), CrI(4275Å) and DI(4339Å). These measurements were made to quantify the relative importance of the wall as a source of impurities.

The line of sight intensity, I, of the observed emission is again given by equation (4.1). For these neutral atoms and low ionisation state ions, I is directly proportional to the neutral impurity influx and the constant of proportionality is a slowly varying function of the edge parameters $n_e(r)$ and $T_e(r)$.

In figure 18 the absolute intensities of DI, CII, OII and CrI are plotted as functions of the line average density. All these lines exhibit similar behaviour. They are much more intense in deuterium than in helium and rise much more rapidly with increasing line average density in deuterium. There is a similarity between this behaviour and that of the radiated power fraction plotted in figure 5.

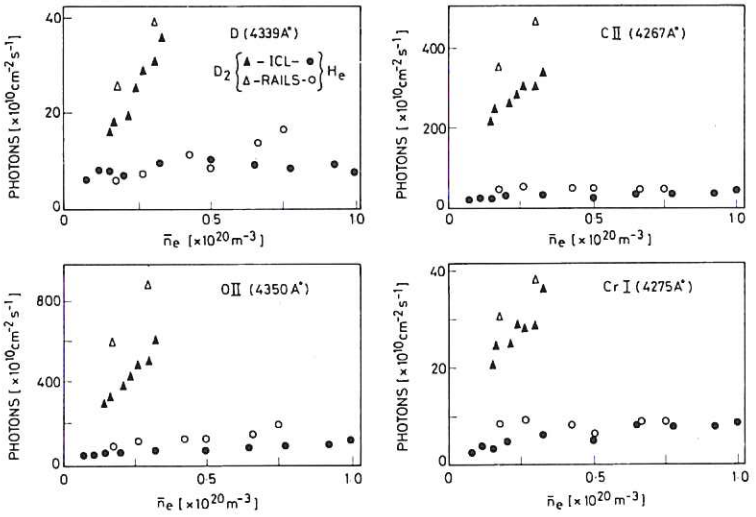

Fig. 18 Line emission in the visible region of the spectrum associated with impurity influxes from the walls. D(4339Å), CII(4267Å), OII(4350Å) and CrI(4275Å) intensities are plotted as functions of line average density.

A simple one-dimensional rate equation model has been used together with experimental edge plasma profiles, to model the impurity influx and line emission processes. The results for oxygen, carbon, chromium and deuterium are listed in table 6. These show that the influxes of oxygen and carbon are three to seven times lower in helium than in deuterium. There is also the suggestion that the influx of carbon is two to three times higher than that of the oxygen in all cases. The influx of chromium is very much smaller than that of the other impurities.

Table 6 Impurity Influxes

	Deuterium		He (low n_e)		He (high n_e)	
	ICL	RAIL	ICL	RAIL	ICL	RAIL
Oxygen OII	7.20^{13}	$1.1x10^{14}$	$1.6x10^{13}$	$2.7x10^{13}$	$6.9x10^{12}$	$6.9x10^{12}$
Carbon CII	$4.6x10^{14}$	$3.5x10^{14}$	$3.3x10^{13}$	$4.9x10^{13}$	$2.5x10^{13}$	$2.5x10^{13}$
Chromium CrI	$4.4x10^{11}$	$5x10^{11}$	$4.8x15^{10}$	$6.4x15^{10}$	$4.8x10^{10}$	$4.8x10^{10}$
Deuterium Dγ/ Hydrogen Hγ	$3.6x15^{14}$	$4x15^{14}$	$9x10^{13}$	$9x15^{13}$	$8x15^{13}$	$1.5x10^{14}$
Fluxes in atoms cm^{-2} s^{-1}						

5. RESULTS: Local Measurements

5.1 Langmuir Probes

The design and disposition of the twelve probes built into the ICL has already been described in section 2. These probes were operated during almost every DITE discharge for the full duration of the pulse. In figure 19 the poloidally averaged electron temperature and density extrapolated to the leading edge of the limiter are plotted as functions of the line average density. Helium and deuterium plasmas have very similar edge densities at a given line average density. However, the electron temperature in deuterium falls much more rapidly with increasing line average density than in helium. In both cases the disruptive density limit is reached when the edge temperature has fallen to between 10 and 15 eV.

Interpretation of individual probe signals from the ICL is difficult due to the significant poloidal asymmetries which were observed with the full

array of probes. With the plasma current in its anti- clockwise direction and the toroidal field clockwise the e-folding lengths on the electron drift side of the ICL were such steeper at the bottom than at the top of the limiter. On the ion drift side the situation was the reverse. This asymmetry was investigated in a series of discharges in which the current and toroidal field were reversed. These experiments showed that the asymmetry could be inverted by changing the sense of the rotational transform but that reversing the plasma current and the toroidal field together resulted in a nearly identical poloidal structure. This

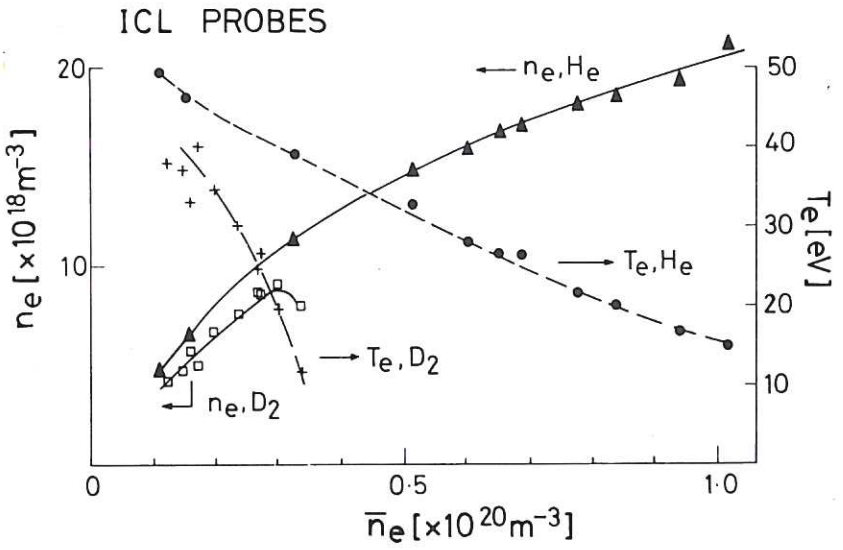

Fig. 19 Poloidally averaged leading edge values of electron density and temperature from the ICL Langmuir probes.

behaviour can be explained by the fact that the ICL was a 180° sector, rather than a full poloidal ring, and that this results in a variation in the connection length as a function of the poloidal position.

Comparisons have been made between the plasma parameters measured with the reciprocating Langmuir probes and the internal ICL probes. The agreement is generally very good although account must be taken of which particular probes are connected on the same magnetic flux tube. In figure 20 the radial profiles recorded by the reciprocating probe array and the ICL are presented, and are in close agreement.

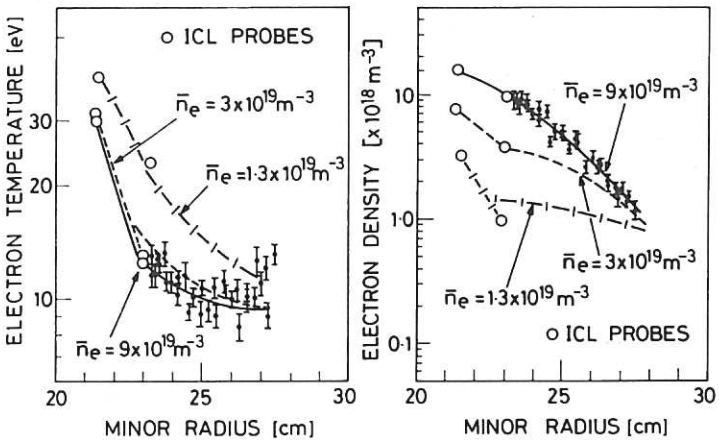

Fig. 20 Comparison of radial profiles from the reciprocating probes and ICL probes.

5.2 CCD Camera Measurements and Code Predictions

Three orthogonal windows were used for viewing the ICL at various stages in the experimental programme; these camera locations are indicated in figures 3 and 4. The key measurements made with the CCD system were the radial distribution of the CI (9050 Å) emission near the ICL and rail limiters. This relates most directly to the original predictions made with the 2D sputtering [1] code. The essential ingredients of this code may be summarised as follows:

(1) The incident ion flux and ion impact energy are calculated at a particular surface element from the local plasma conditions.

(2) A physical sputtering yield is computed for the specified surface atoms and incident plasma species [6].

(3) Trajectories for the sputtered atoms are generated at each element of surface with a Thompson distribution of angles and energy [7].

(4) The ionisation is calculated in each cell of the plasma grid intersected by a trajectory.

The only refinement to the code necessary for the comparison with the CCD data is the computation of the CI emission. This requires a knowledge of the photon efficiency which is defined as the number of ionisation events per photon. The absolute value of this parameter is not very well known

but its scaling with electron temperature is fairly reliable. We assumed a linear dependence of the photon efficiency with electron temperature [8].

In making a comparison between the rail limiters and the ICL the tangential windows were used, since these provided equivalent views. A digital frame store was employed when generating contour plots of emission from particular frames of interest. Contours of CI in the vicinity of the ICL and top rail limiter when viewed from the tangential windows are shown in figure 21 with the outline of the limiters sketched in. The striking feature of the contours for the ICL is that the emission is peaked in the SOL and there is very little emission from the concave surfaces of the ICL tiles.

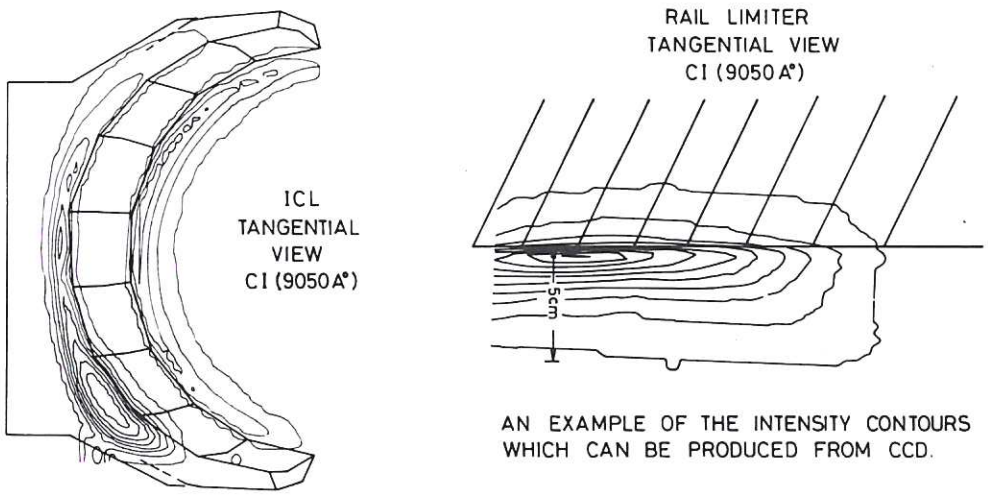

Fig. 21 CI (9050Å) emission contours for the ICL and rails recorded with the tangentially viewing CCD camera system

Plasma parameters which were required as input for the code were obtained from the Langmuir probe measurements. In the case of the ICL, data from the internal probes was used and for the rail limiters the necessary profiles were obtained with the reciprocating probes. In figure 22 a comparison is made between the CCD camera data for the radial distribution of CI and the code predictions for both the rail limiters and the ICL in a helium plasma. Theory and experiment are in good agreement considering that there are no arbitrary parameters to adjust. As predicted the CI emission produced by the ICL is strongly localised in the scrape-off layer. This is in complete contrast to the rail limiter case where the bulk of the emission comes from inside the limiter radius.

If the CI profiles recorded at a range of densities in helium plasmas are normalised, and plotted on the same scale there is no significant difference between them. The CI profiles predicted by the code are also very insensitive to line average density. This seems to result from the coupling between the edge temperature and density [10].

In calculating the CI emission from the ICL an effective tip radius of 1 mm was specified. All the tiles were finished with a 0.5 mm flat at the leading edge but we have assumed that the ion Larmor radius will effectively increase this by another 0.5 mm. If a perfectly sharp leading edge is assumed the emission from inside the limiter radius is much too low.

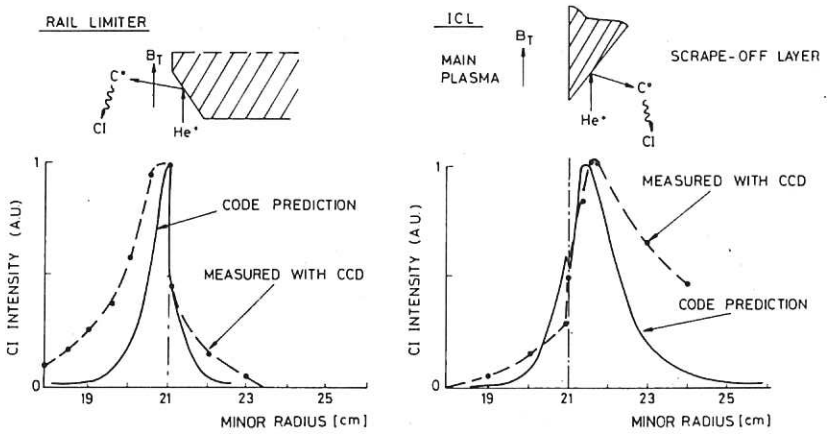

Fig. 22 Predicted and measured radial distributions of CI for the ICL and rail limiters (Helium, $\bar{n}_e = 5 \times 10^{19}$ m^{-3}).

The CCD camera mounted on the rear of the ICL drive box, shown in figure 3, was able to view the tiles near the mid-plane out to the leading edges. Data obtained from this source has been digitised and integrated over an area corresponding to that of one of the single tiles containing Langmuir probes. In figure 23 the integrated CI intensity is plotted as a function of line average density for a helium discharge. A prediction of this data has also been made using the density scaling of the edge plasma parameters, measured with the Langmuir probes, as input for the sputtering code. The solid lines which are also plotted in figure 23 show the result of this procedure. An arbitrary normalisation has been used in fitting the code results to the data but the predicted density scaling is consistent with the observations. The reason for the decrease in CI intensity at higher density is that although the particle flux incident on the ICL increases with the line average density the electron temperature falls. This decline in edge temperature reduces the sputtering yield of the plasma ions at a faster rate than the increase in incident flux and as a result the total

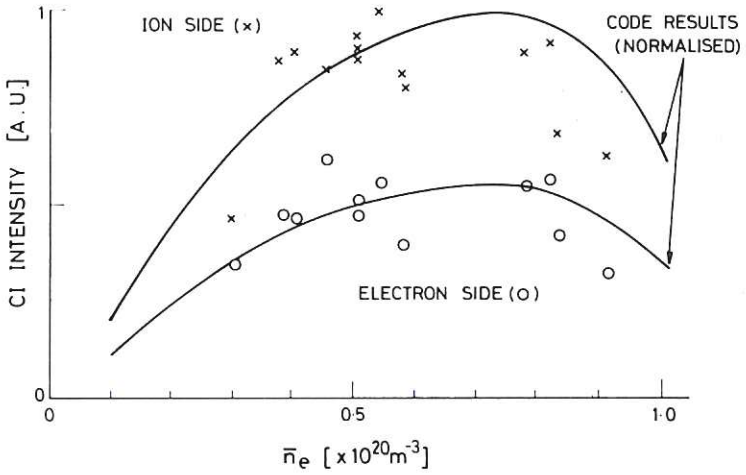

Fig. 23 Comparison of measured and predicted integrated CI intensities versus line average density for helium discharges.

influx of carbon decreases. In addition the photon efficiency and screening factors, which are included in the code, are also affected by the plasma edge parameters.

5.3 Collector Strips

Nickel and carbon samples were mounted in holders behind ICL tile 4. These were intended to collect any neutral impurities, in particular carbon, deposited during the period of operation. Since the replacement of the collector strips would have required a vacuum opening of the torus, they were left in position for the whole duration of the experiment. In many applications this integration over many shots, coupled with uncertainties about the plasma conditions, makes interpretation of the results problematical. However, in this experiment Langmuir probe data was recorded on almost every shot and the discharge parameters were well controlled and documented. As a result a very good estimate of the total fluence to the ICL tile facing the collector could be obtained.

The main objective of analysing the collector strips was to test the predictions of the deposition of the sputtered neutral carbon which was not ionised by the SOL plasma. Three methods of analysis were used to determine the carbon film thickness:

(1) Brightly coloured interference fringes were clearly visible on all the collectors. The number and colour of these fringes were used to estimate the carbon film thickness [9].

(2) Rutherford backscattering (RBS) was used to determine the surface concentrations of oxygen and iron on the carbon samples. A broadening

of the peaks in the RBS spectrum results from the finite film thickness. Since the iron and oxygen prove to be minor constituents of this film, the carbon concentration is readily calculated.

(3) A direct measure of carbon concentration on the nickel samples was obtained with auger electron spectroscopy (AES). Depth profiling in this case was achieved by sputter erosion of successive layers of the carbon film.

The total carbon deposition measured by each of the above techniques is plotted as a function of distance along the collector in figure 24. All of these measurements are in very close agreement. Also shown in the same figure is the carbon deposition predicted by the 2-D sputtering model. This prediction required input data in the form of suitable plasma conditions and a normalisation factor to allow for integration over all the discharges. The ion fluence for each discharge, measured by Langmuir probes, was roughly proportional to line average in all discharges studied. Total fluence of plasma ions to the tile nearest to the collectors was estimated from the product of the fringe count summed over all discharges and the mean fluence per fringe (8×10^{19} m^{-2} f^{-1}). During the period of operation there were a total of 147 helium discharges with an average density of 5.1×10^{19} m^{-3} and 105 deuterium shots with a mean density of 2.4×10^{19} m^{-3}. In normalising the code result the deuterium discharges were ignored. This is because not only was the fluence of deuterons only 30% of the helium fluence but also the electron temperature, and hence the sputtering yield, was much lower in deuterium plasmas. It should also be noted that in the simulation we have assumed that the majority ions are He^{+}. If most of the ions were He^{++} this would halve the fluence but at the same time, the ion impact energy is nearly twice as big and this nearly doubles the sputtering yield under average conditions. The approximation that 100% of the incident ions are He^{+} therefore results in only a small error.

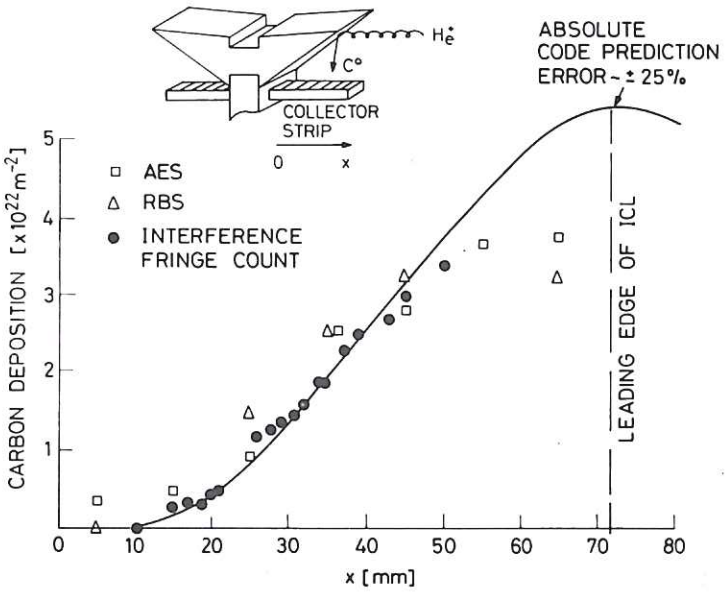

Fig. 24 The thickness of the carbon film deposited on a collector underneath an ICL tile from a variety of measurements and the code prediction.

The exact passage of the line predicted by the code through the points from the surface analysis may be partly fortuitous but even so, changes in the assumptions used in the normalisation are unlikely to cause more than a 25% displacement of the curve. Qualitatively there is also good agreement between the shape of the predicted deposition and the measurements. However, there is some discrepancy near the leading edge of the ICL where the code result is too high. At present we have no definitive explanation of this difference, although it might be attributed to an erosion of the deposited layer involving sputtering by backscattered helium ions.

The RBS analysis also showed that the carbon film deposited on the collectors contained 2% iron and 10% oxygen. Such a high concentration of oxygen is almost certainly a genuine result of bombardment from the plasma and not an oxidation of the iron after exposure to the atmosphere. This supports the conclusion reached by the spectroscopic study that the oxygen is a major contributor to the impurity content of these discharges, whereas iron is not.

6. MODELLING THE EDGE ELECTRON TEMPERATURE

A simple model which has successfully reproduced the scaling of edge electron temperature with line average density on JET [10] has been applied to the ICL discharges. This model assumes that the impurity source which dominates the total radiated power in a tokamak is the carbon which is physically sputtered from the limiters. An iterative procedure is used which contains the following steps:

(1) As input we need to know the line average density at which we want to calculate the edge temperature and a guess at the value of this temperature. We then use an empirical relationship to give us the total ion flux to the limiter at the line average density which we have chosen. In the case of the DITE data a linear scaling which is roughly consistent with the Langmuir probe data of figure 10 (a) was chosen.

(2) Since we know the ion flux and the electron temperature we can now calculate the energy of the incident ions and hence the total flux of physically sputtered neutral carbon atoms. Combining the electron temperature and the incident flux we can also calculate the edge electron density.

(3) We have now specified the edge plasma conditions and the total carbon influx, the next step is to estimate the resulting impurity content of the plasma. In the model this is done on the basis of an analytical solution to the one dimensional diffusion equation which was originated by Engelhardt [11]. This gives us the central carbon density in terms of the neutral impurity mean free path and the influx.

(4) Now we convert the impurity density into an estimate of the total radiated power using the assumption that it is proportional to the product of the electron and impurity densities but is independent of electron temperature. This is a reasonable approximation provided that the impurity is not in coronal equilibrium [12].

(5) Any of the input power which is not radiated is transported to the scrape-off layer and is convected to the limiter. Since the power deposited on the limiter is proportional to the product of the flux and the electron temperature we are free to adjust the electron temperature to a value which gives us a convected power equal to the difference between the input and radiated powers.

(6) If the last step has resulted in a significant adjustment to the electron temperature we must return to step 2 to recalculate the sputtered influx. Iteration of the electron temperature continues until self consistency is achieved.

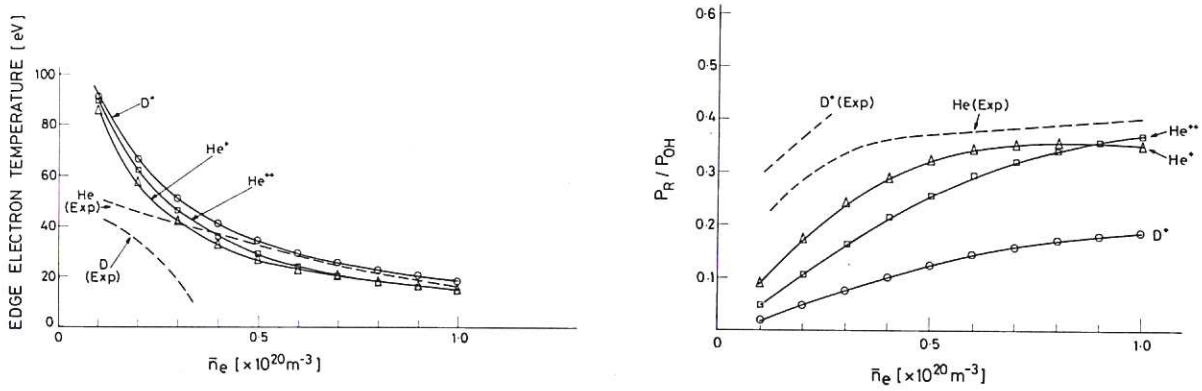

Fig. 25 Self consistent code prediction of (a) edge temperature T_e, and (b) P_R/P_{OH}, versus $\bar{n}_e$ in D_2 and He plasma compared with the experimental results.

Figure 25(a) shows a comparison between the radiated power fraction P_R/P_{OH} predicted by the model and the experimental results. In the case of helium the model successfully reproduces the general form of the density scaling; P_R/P_{OH} rises almost linearly with the average density at low density and flattens off at high density. This behaviour results from the form of the yield curve for the physical sputtering of carbon which varies strongly with energy at low ion energies and flattens off at high ion energy. The predicted scaling of the edge electron temperature for helium is also qualitatively correct and is shown in figure 25(b). In all cases the deuterium data is poorly fitted by the model.

These results are most relevant to the discussion of the relative importance of the wall fluxes. The model is not sufficiently refined to take the screening provided by the ICL into account.

7. SPUTTERING CODE PREDICTIONS

In section 5.2 we summarised the processes which are included in the two dimensional sputtering model which was used in the original evaluation of limiter geometries. In addition to the calculation of the toroidal and radial distributions of the C^+ ion source, the code contains a one dimensional radial transport model based on diffusion alone [1]. Although this is not expected to give accurate absolute numbers, the predictions for the relative performance of different limiter geometries should be adequate.

In the absence of any simple description of the toroidal transport of the ionised impurities in the plasma boundary, two options are available in the code which set rough limits on the results. We can either assume that the neutral impurities ionised in the scape-off layer disperse toroidally, creating a uniform cylindrical shell, or that carbon ions created in the scrape-off layer are rapidly driven back to the limiter by friction with the hydrogenic ions. In this latter case we can ignore all ionisation occurring outside the limiter radius.

Using the plasma parameters recorded by the Langmuir probes within the ICL, the code has been run for both the rail limiter and ICL geometries in helium plasmas. It was decided to use the same plasma conditions in both cases because of the uncertainties associated with the rail limiter scrape-off layer. In figure 26 the predicted central carbon density is plotted as a function of line average density. When the ionisation in the scrape-off layer is included (SOL C^+ on), the ICL is expected to reduce the carbon content of the discharges by a factor of 2.2 to 3.5, depending on the line average density. With the ionisation in the scrape-off layer excluded (SOL C^+ off) the range is from 3.3 to 5.3. A constant value for the cross-field diffusion coefficient of $D = 1\ m^2\ s^{-1}$ was assumed in all cases, consistent with our original paper [1].

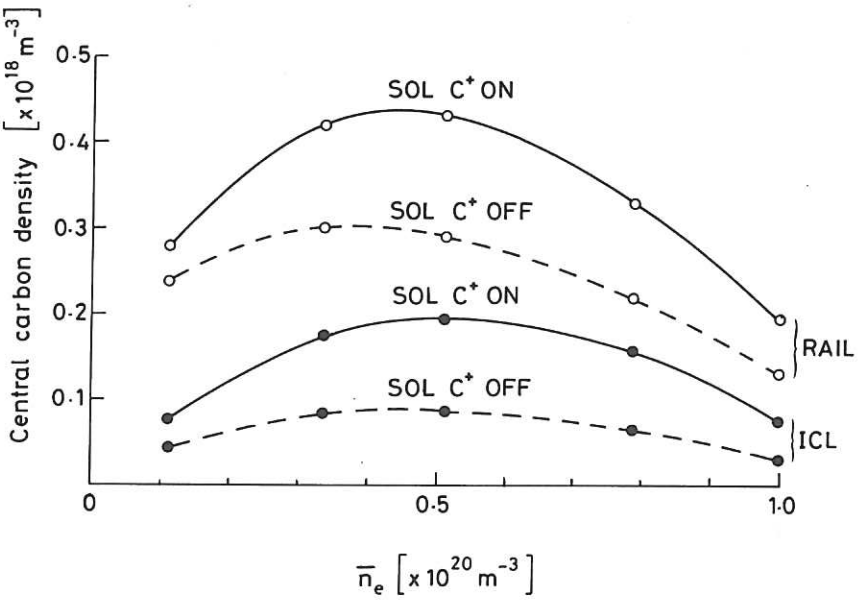

Fig. 26 Two-dimensional sputtering code predictions for the central carbon impurity density for the rail and ICL limiters. Ionisation in the scrape-off layer can be included (SOL C^+ on), or excluded (SOL C^+ off) from the transport calculations.

8. DISCUSSION

8.1 Global impurity control

The ambitious objectives of the ICL have been rewarded by a fair measure of success. A substantial reduction of the impurity radiation (50%) has been demonstrated in helium plasma but was not as great in deuterium (20%).

An analysis of the temperature profile, measured with the Thomson scattering system, indicates that the ICL reduces the Z_{eff} in the helium discharges (3.5 to 2.5 at a line average density of 3×10^{19} m^{-3}). The temperature profiles in all the discharges studied, low and high density deuterium or helium with the rails or ICL, were almost indistinguishable. However, the loop voltage was always reduced by the ICL.

Predictions have been made for the relative carbon content of the rail and ICL discharges using a two-dimensional sputtering code coupled to a one-dimensional impurity transport model. Using measured edge plasma parameters as input these calculations indicate that the ICL should reduce the carbon impurity density by a factor in the range 2 to 5. This performance is not as good as we predicted in our original paper [1], but the edge plasma parameters used in these calculations were significantly different from those which we measured in the experiment.

8.2 The dominant impurity species

Spectroscopic measurements, when coupled with a one-dimentional transport code, indicate that the oxygen and carbon impurities are responsible for the majority of the radiated power loss, each typically accounting for around 50% of it. Calculations of the iron concentration show that it only accounted for around 1% of the total radiation. However, the density dependence of the central iron concentration did suggest that it was responsible for the soft X-ray emission.

8.3 The role of wall produced impurities

Strong evidence for the important role played by wall produced impurities is provided by the contrasting behaviour of deuterium and helium discharges. The disruptive density limit in helium plasmas was found to be almost three times higher than in deuterium. It seems probable that this difference is associated with the influx of impurities from the walls which was measured to be between three and seven times higher in deuterium than

in helium at a given line average density. The contributions to the total radiated power estimated from observation of the higher ionisation states of carbon and oxygen are significantly higher in deuterium plasmas. We associate these differences in behaviour with the charge exchange flux, which is measured in ASDEX [13] to be 5-15 times higher in deuterium than in helium. However, in this paper it is concluded that when the energy distributions are included, the energy dependence of the physical sputtering yields is such that it cancels out the effect of the increased flux. It therefore seems likely that the influx of impurities from the vessel walls in DITE results either from a desorption of the gaseous impurities which is induced by the flux of charge exchange neutrals, or the release of molecules produced as a result of chemical reactions involving hydrogen at the wall surfaces.

Further evidence which supports the argument that physical sputtering by charge exchange particles does not usually dominate comes from the neutral transport code DEGAS. Using conditions appropriate to DITE [14], these calculations have shown that the total flux of neutrals to the wall does not exceed the ion flux to the limiters and that the average energy of the neutrals is lower than that of the ions striking the limiter. When screening by the scrape-off layer is also considered, it is difficult to understand how, with physical sputtering alone, the wall could ever be other than of secondary importance in impurity production to the limiters.

The total neutral atom influx from the walls can be estimated by multiplying the specific influxes listed in table 6 by the internal surface area of the DITE torus (1.3×10^5 cm^2). This can then be compared with the code predictions for the influx of neutral carbon physically sputtered from the limiters (section 5.2). In a helium plasma at a line average density of 3×10^{19} m^{-3}, the total influx of carbon impurities from the walls is estimated to be 4×10^{18} s^{-1} whilst that from the ICL is 6×10^{19} s^{-1}. Helium plasmas would therefore be expected to be limiter impurity dominated. The comparable deuterium discharge at the same line average density yields a total wall carbon influx of 3×10^{19} s^{-1}, and a limiter source of 2.5×10^{19} s^{-1}. These deuterium discharges are therefore expected to be strongly influenced by impurities originating from the walls, which would explain why the ICL is most effective in helium where the wall sources are much less significant.

8.4 Local Interactions

The interaction of the ICL with the edge plasma seems well understood. Good agreement is found between the predicted and measured spatial distributions of the CI emission in the vicinity of the rail limiters and ICL. The distribution and absolute thickness of the carbon deposit

collected on samples placed beneath the ICL tiles has been accurately modelled by a two-dimensional computer code. The scaling of the total CI emission with line average density also agrees with the code predictions. This consistency between the experiment and theory demonstrates that the physical assumptions that the model contains such as sputtering yields, energy distribution of sputtered atoms, ionisation rate coefficients and photon efficiency are fairly accurately described. Since the spectral lines we have observed are from neutral atoms the plasma can be treated merely as a target into which these atoms are launched. This avoids all the uncertainties and complications associated with the transport of ionised species.

8.5 Thermal Response

So far we have not mentioned the problem of the thermal loading of the leading edge of the ICL. This has been carefully studied theoretically with a finite element code and experimentally using an infra-red camera. The results are described elsewhere [15]. Our conclusion is that the thermal response of the ICL is similar to that of a semi-infinite solid heated uniformly on its face.

8.6 The Edge Plasma Model

Results were presented in section 5 from a model which uses the edge electron temperature for feedback between the core plasma and the physical sputtering of carbon impurity from the limiter. The predicted edge electron temperature and total radiated power have a dependence on line average density which corresponds well with measurements made in helium plasmas. In deuterium discharges the model does not agree at all well with the experimental data. This failure provides further support for the view that the discharges in deuterium are essentially wall impurity dominated.

8.7 Spectroscopy

Spectroscopy was applied in these experiments with the main objective of demonstrating a reduction in the carbon content of the discharge as a result of the ICL geometry. Since the ICL produced a halving of the total radiated power and a lowering of the loop voltage in helium plasmas it was hoped that the observations of the higher ionisation states would identify which impurity was responsible. In general the higher the ionisation state of the ions under study the more reliable is the interpretation. This is because these ions radiate from toroidally and poloidally uniform shells

relatively close to the plasma core where the impurity confinement time is long and an approach to coronal equilibrium is assured.

Measurements made of the OVIII line, which has its maximum intensity within 8cm of the plasma centre, have shown that the oxygen content of the helium discharges is reduced by a relatively small factor when the ICL is introduced. The OVI line which is expected to have its peak emission 1cm inside the limiter behaves very differently but we are able to discount it on the grounds of toroidal non-uniformity. Iron can be discounted as major contributor to the total radiation since observations of FeXVII, which peaks at a minor radius of 5cm, indicate that the iron concentrations are low. This leaves us with the carbon which could not be observed close to the plasma core. Calculations based on the CV line measurements showed a small reduction in the radiation from carbon in helium plasmas, not exceeding 30%, and no effect in deuterium. We are therefore left with the problem that the spectroscopic measurements are qualitatively but not quantitatively consistent with the bolometer data.

A consistent spectroscopic picture is however obtained for the change over from helium to deuterium in either ICL or rail limiter discharges. Observations of the low ionisation states, which correspond to impurity influxes from the walls show that the carbon and oxygen influxes are dominant in deuterium plasmas but not in helium.

9. CONCLUSION

All local measurements made in the vicinity of the ICL indicate that it behaved as originally predicted. Significant reductions in loop voltage and total radiation have been achieved in helium plasmas. In deuterium reductions are also observed at a lower level. All the evidence suggests that that the limiter dominates as an impurity source in helium, but is comparable to the wall sources in deuterium. Spectroscopy of the higher ionisation states shows that the ICL reduces the carbon, oxygen and iron impurities. However, these reductions are not quantitatively consistent with the change in total radiation recorded by the bolometers. This may be associated with the lack of suitable spectral lines for observing carbon near the centre of the discharge and the problem of interpreting the emission from lower ionisation states nearer the periphery.

ACKNOWLEDGEMENTS

We wish to thank all members of the DITE team for their help and cooperation and Dr Behringer for the use of his computer code.

REFERENCES

[1] G F Matthews, G M McCracken, P C Stangeby, C S Pitcher, P Sewell, D H J Goodall, Plasma Physics and Controlled Fusion, Vol 29, No 2 (1987) 189-203.

[2] K H Finken, K H Dippel, D Peiter, G H Wolf, G A Campbell, R W Conn, D M Goebel, W K Leung, G J Thomas, A E Pontau, Journal of Nuclear Materials, vols 145-147 (1987) 825-829

[3] C S Pitcher, Journal of Vacuum, Science and Technology A., Vol 5, Issue 3, (1987) 383.

[4] J Hugill, Private Communication, 1987

[5] K H Behringer et al, Nuclear Fusion, Vol 26, No 6 (1986) pp 751-768

[6] J Bohlansky, Nuclear Fusion Data Compendium for Plasma Surface Interactions (1984) 55-72

[7] M W Thompson, Physics Reports, Vols 69 (1981) 335.

[8] I I Sobelman, L A Vainshtein, E A Yukov, Excitation of Atoms and Broadening of Spectral Lines, Springer Series in Chemical Physics 7 (Springer, Berlin, 1981)

[9] P Wienbold, U Littmark to be published in Journal de Physique

[10] G M McCracken, Plasma Physics and Controlled Fusion (to be published)

[11] W Engelhardt, W Feneberg, Journal of Nuclear Materials, vol 76, (1978) 518.

[12] P G Carolan, V A Piotvowicz, Plasma Physics, vol 25, No 10 (1983) 1065-1086.

[13] H Verbeck and the ASDEX team, Journal of Nuclear Materials, vols 145-147, (1987) 523.

[14] G P Maddison, J Allen, S J F Fielding, P C Johnson, G F Matthews, Journal of Nuclear Materials, vols 145-147, (1987) 534.

[15] D H J Goodall, G F Matthews, G M McCracken, C S Pitcher, D A Hughes, 14th European Conference on Controlled Fusion and Plasma Physics (Madrid 1987) Vol 11D Part II P766.

Available from
HER MAJESTY'S STATIONERY OFFICE
49 High Holborn, London, WC1V 6HB
(Personal callers only)
P. O. Box 276, London, SE1 9NH
(Trade orders by post)
13a Castle Street, Edinburgh, EH2 3AR
41 The Hayes, Cardiff, CF1 1JW
Princess Street, Manchester, M60 8AS
Southey House, Wine Street, Bristol, BS1 2BQ
258 Broad Street, Birmingham, B1 2HE
80 Chichester Street, Belfast, BT1 4JY

PRINTED IN ENGLAND